HEP-19-2399

Lipid remodelling in hepatocyte proliferation and hepatocellular carcinoma

Zoe Hall[1,2,*], Davide Chiarugi[3], Evelina Charidemou[1], Jack Leslie[4], Emma Scott[4], Luca Pelligrinet[1], Michael Allison[5], Gabriele Mocciaro[1], Quentin M. Anstee[4,6], Gerard I. Evan[1], Matthew Hoare[5, 7], Antonio Vidal-Puig[3], Fiona Oakley[4], Michele Vacca[1,3,#,*] & Julian L. Griffin[1,2 ,#, *]

[1] Department of Biochemistry and Cambridge Systems Biology Centre, University of Cambridge, Cambridge, United Kingdom; [2] Biomolecular Medicine, Division of Systems Medicine, Department of Metabolism, Digestion and Reproduction, Imperial College London, London, United Kingdom; [3] Metabolic Research Laboratories, Wellcome Trust-MRC Institute of Metabolic Science, Cambridge, United Kingdom; [4] Institute of Cellular Medicine, Faculty of Medical Sciences, Newcastle University, Newcastle upon Tyne, United Kingdom; [5] Department of Medicine, Addenbrooke's Hospital, Cambridge Biomedical Research Centre, Cambridge, United Kingdom; [6] Newcastle NIHR Biomedical Research Centre, Newcastle upon Tyne Hospitals NHS Foundation Trust, Newcastle upon Tyne, United Kingdom; [7] CRUK Cambridge Institute, Robinson Way, Cambridge, United Kingdom

[#] Equal contribution; * Corresponding author

Keywords:

liver regeneration; cancer metabolism; mass spectrometry imaging; HCC; phosphatidylcholine

Corresponding Author Contact Information:

Dr Zoe Hall; Biomolecular Medicine, Department of Metabolism, Digestion and Reproduction, Sir Alexander Fleming Building, South Kensington Campus, Imperial College London, Exhibition Road, London SW7 2AZ, United Kingdom; zoe.hall@imperial.ac.uk; Tel.: +44 (0) 7709 844249.

Dr Michele Vacca; Metabolic Research Laboratories, Wellcome Trust-MRC Institute of Metabolic Science, Box 289, Addenbrooke's Hospital, Cambridge CB2 0QQ, United Kingdom; mv400@medschl.cam.ac.uk; Tel.: +44 (0) 7474 301485

Professor Julian L. Griffin; Biomolecular Medicine, Department of Metabolism, Digestion and Reproduction, Sir Alexander Fleming Building, South Kensington Campus, Imperial College London, Exhibition Road, London SW7 2AZ, United Kingdom; julian.griffin@imperial.ac.uk; Tel: +44 (0)20 7594 3220.

List of Abbreviations:

HCC – Hepatocellular carcinoma

PC – Phosphatidylcholine

NAFLD – non-alcoholic fatty liver disease

NASH – non-alcoholic steatohepatitis

CTNNB1 - β-catenin

PH - partial hepatectomy

CCl_4 - carbon tetrachloride

PB - phenobarbital

DEN - N-diethylnitrosamine

HFD - high fat diet

LC-MS – liquid chromatography mass spectrometry

MSI - mass spectrometry imaging

PCA - principal components analysis

PLS-DA - partial least squares discriminant analysis

OPLS-DA -orthogonal projection to latent structures discriminant analysis

SEM – standard error of the mean

PCNA - proliferating cell nuclear antigen

NGS - Next Generation Sequencing

IPA - Ingenuity Pathway

FBA - flux balance analysis

GEM - genome-scale metabolic model

PPARα - nuclear receptor peroxisome proliferator-activated receptor α

MUFA - monounsaturated fatty acid

PUFA - polyunsaturated fatty acid

SFA – saturated fatty acid

PE - phosphatidylethanolamine

TAG – triacylglyceride

FFA - free fatty acid

SM - sphingomyelin

TCA - citric acid cycle

ACSL - long chain acyl-CoA synthetase

SCD – stearoyl coA desaturatase

Financial Support:

J.L.G., Z.H. and M.V. are funded by the Medical Research Council (MRC grant MC UP A90 1006 & MC PC 13030). J.L.G. and Z.H. are supported by the Imperial Biomedical Research Centre, NIHR. M.A., A.V-P., F.O., Q.M.A. and M.V. are members of the EPoS consortium, which is funded by the Horizon 2020 Framework Program of the European Union under Grant Agreement 634413. F.O. is supported by MRC program grants (MR/K0019494/1 and MR/R023026/1). J.L is supported by MRC PhD studentship and a CRUK program grant (C18342/A23390). M.V. and A.V-P. are supported by MRC MDU and MRC DMC (MC UU 12012/2). Q.M.A. received additional research support from The Liver Research Trust and is a Newcastle NIHR Biomedical Research Centre investigator. M.A., M.V., A.V-P. and J.L.G. received research support from the Evelyn Trust and the NIHR Cambridge Biomedical Research Centre (Gastroenterology Theme).

ABSTRACT

Background & Aims: Hepatocytes undergo profound metabolic rewiring when primed to proliferate during compensatory regeneration and in hepatocellular carcinoma (HCC). However, the metabolic control of these processes is not fully understood. In order to capture the metabolic signature of proliferating hepatocytes, we applied state-of-the-art systems biology approaches to models of liver regeneration, pharmacologically- and genetically-activated cell proliferation, and HCC.

Approach & Results: Integrating metabolomics, lipidomics and transcriptomics, we link changes in the lipidome of proliferating hepatocytes to altered metabolic pathways including lipogenesis, fatty acid desaturation, and generation of phosphatidylcholine (PC). We confirm this altered lipid signature in human HCC and show a positive correlation of monounsaturated-PC with hallmarks of cell proliferation and hepatic carcinogenesis.

Conclusion: Overall, we demonstrate that specific lipid metabolic pathways are coherently altered when hepatocytes switch to proliferation. These represent a source of targets for the development of new therapeutic strategies and prognostic biomarkers of HCC.

INTRODUCTION

The liver is characterised by an impressive regenerative potential following cell loss or the activation of direct hyperplasia programs. Compared to other organs and tissues, where the regeneration is mainly driven by stem cell precursors, liver regeneration often requires the proliferation of differentiated hepatocytes to compensate for cell loss (1). Aberrant hepatocyte proliferation in chronic liver disease is also a driving cause of hepatocellular carcinoma (HCC), one of the leading causes of cancer-related deaths world-wide. HCC typically occurs on a background of chronic liver disease, with risk factors including viral or autoimmune hepatitis, chronic alcohol abuse, and non-alcoholic fatty liver disease (NAFLD) (2, 3). HCC is genetically heterogeneous, with mutations in the *TERT* promoter, *TP53* and *CTNNB1* (β-catenin) most frequently reported (4). Whilst more commonly preceded by cirrhosis, HCC may also develop directly in a context of non-alcoholic steatohepatitis (NASH) (5). The pathogenesis of fatty liver-associated HCC is complex and the focus of intense research. Some of the contributing factors are thought to include hepatic lipotoxicity, oxidative stress, modulation of nuclear receptors, stellate cell activation, and the chronic activation of wound-healing processes including inflammatory and immune responses, together producing a carcinogenic *milieu* (6-8).

One of the hallmarks of HCC, and cancer in general, is cellular proliferation. In order to fuel this proliferation, there is a higher demand for macromolecular biosynthesis, for structural and energy purposes. There is also a need to evade the consequences of a deleterious environment (e.g. hypoxia and reactive oxygen species), and thus extensive metabolic reprogramming occurs in cancer cells (9-12). Increased uptake and utilisation of glucose via glycolysis (the Warburg effect), increased fatty acid uptake and increased *de novo* lipid synthesis have all been described (13, 14). It is widely accepted that many molecular and metabolic mechanisms are partially conserved between liver regeneration and HCC (15). Despite the importance for normal wound healing and its relevance to HCC, very little has been reported on the metabolic alterations of regenerating hepatocytes,

particularly with respect to lipid-related pathways (16-19). Characterising the metabolic remodelling that hepatocytes undergo during compensatory regeneration and in HCC is thus crucial to identify metabolic pathways that relate to cell proliferation in general and, more specifically, to HCC growth.

To bridge this gap, we used a multi-omics approach to characterise the metabolic rewiring of hepatocytes in proliferation, for a range of mouse models of liver regeneration, hepatic hyperplasia and HCC. Overall our findings shed new light on the lipid-related metabolic adaptations occurring in cell proliferation and survival, highlighting a coherent role of lipid composition and lipid pathways in the context of liver regeneration and cancer.

EXPERIMENTAL PROCEDURES

Animal studies

All data are from male C57BL/6 mice purchased from Charles River (Edinburgh, U.K.) or MRC Harwell Institute (Harwell, U.K.). Mice were housed in a temperature-controlled room (21°C) with a 12-hour light/dark cycle with free access to diet and water. The UK Home Office and the Bioethics Committees of the Universities of Cambridge and Newcastle approved all animal procedures. Mice were fed on a chow diet (Safe Diets, Code ds-105) unless otherwise stated in the description of the different procedures.

Partial hepatectomy: Twelve week-old mice underwent two-thirds partial hepatectomy (PH) procedure, according to the method of Higgins and Anderson (20). The left lateral and median lobes were completely excised. Mice were sacrificed 3 days after hepatectomy to mimic the peak of proliferation. Resected livers were used as time 0 control for gene and lipid analyses to perform paired analyses (N = 5 per group).

Carbon tetrachloride studies: Sixteen week old mice were maintained as specific pathogen free according to the FELASA Guidelines and underwent IP injection of 2 μL/g body weight of CCl_4 : olive

oil (1:1 v/v) mix, or olive oil only (N = 3 per group). Mice were humanely culled under isofluorane terminal anaesthesia, 3 days after the IP injection.

Phenobarbital: Pharmacologically-induced hepatocyte proliferation was induced in mice (18-20 weeks old) by the administration of 0.1% phenobarbital (PB) in drinking water for 72 hr, before humane culling (N = 5 or 6 per group).

N-Diethylnitrosamine-induced HCC: Two week-old mice were given a single IP injection of N-diethylnitrosamine (DEN) (30 mg/kg) and were maintained on a chow diet for a further 40 weeks (N = 4) or a high fat diet (HFD; D12331, Research Diets Inc with 58 kcal% fat and sucrose) for a further 30 weeks (N = 6). Mice fed a HFD were also given 42.1 g/L of sugar (18.9 g glucose and 23.0 g of fructose) in their drinking water.

Oncogenic model of HCC: In a genetic mouse model of HCC, activation of *Kras* and *Myc* oncogenes in sporadic hepatocytes and subsequent tumour formation, was achieved in *Kras^{G12D}-RosaMycER* animals (21, 22) *i.v*. delivery of AAV8-TBG-CRE virus (Vector Biolabs, Malvern, PA) and daily *i.p.* tamoxifen (Sigma Aldrich, St. Louis, MO) delivery for 2 weeks.

Human samples

Seven patients undergoing liver transplantation for HCC, developing in a cirrhotic fatty liver (NASH, N=2; alcohol-related liver disease, N=5; **Table S1**) background were recruited at Addenbrooke's Hospital, Cambridge (Division of Hepatology). All the patients had HCC and tumour-free background liver tissue collected. Histological analysis was performed by the Department of Pathology, Addenbrooke's Hospital, and snap-frozen tissue was stored at -80 °C for research purposes in the Cambridge Human Tissue Bank. The study protocol was approved by the Office for Research Ethics Committees of Northern Ireland (LREC 16/NI/0196). All patients gave their informed consent for the use of clinical data and samples for scientific research purposes. The principles of the Declaration of Helsinki were followed.

Lipid and metabolite profiling

Lipids and metabolites were extracted from tissue using the Folch method (23). Briefly, 30 mg of liver tissue was homogenised in chloroform: methanol (2:1, 1 mL) using a TissueLyser (Qiagen Ltd., Manchester, UK). Deionised water (400 μL) was added, and the samples well mixed. Separation of the aqueous and organic layers was carried out following centrifugation (12,000 *g*, 10 min). The resulting organic and aqueous extracts were dried-down under nitrogen or in a vacuum centrifuge, respectively and stored at -80 ^{o}C until analysis.

The organic lipid-containing layer was analysed by untargeted liquid chromatography-mass spectrometry (LC-MS) using an Accela Autosampler coupled to a LTQ Orbitrap Elite^{TM} (Thermo Fisher Scientific, Hemel Hempstead, UK). Lipid identification was performed by accurate mass using an in-house database. The aqueous fraction was analysed by targeted LC-MS/MS using UHPLC+ coupled to a TSQ Quantiva mass spectrometer (Thermo Fisher Scientific, Hemel Hempstead, UK). The mass spectrometer was operated in SRM mode; transitions and source conditions for each metabolite are summarised in **Table S2.** Further method details are available in the supporting information.

RNA extraction

RNA was isolated using miRNAeasy Mini Kits (Qiagen), according to the manufacturer's instructions. Samples were stored at - 80°C prior to use. All reagents and consumables used were nuclease free (molecular biology grade). RNA purity (A260/A280 > 1.80) and concentration were determined using Nanodrop (Thermo Fisher scientific, Delaware USA). RNA integrity was studied using the 2100 Bioanalyzer System (Agilent) and RNA 6000 Nano Kit.

Whole transcriptome amplification and RNA sequencing

RNA from tissues of murine (2 μg RNA) or human (1 μg RNA) were used to generate barcoded sequencing libraries using the TruSeq® Stranded mRNA Library Preparation Kit (Illumina) or TruSeq Stranded total RNA Library Preparation Kit for murine and human liver, respectively, following

manufacturer's instructions. The sequencing libraries were normalized for concentration and combined into pools. The libraries were sequenced using an Illumina HiSeq 4000 instrument at single-end 50bp (SE50) or NextSeq 500 at single-end 75bp (SE75), equivalent to > 20 million reads per sample.

Bioinformatics functional analyses

Pathway enrichment was investigated for differentially expressed genes within groups using Ingenuity Pathway Analysis (IPA, Qiagen). Canonical pathways, Bio-functions, and Upstream Regulators analyses were generated by imputing "biologically significant" genes [statistically significant (q score < 0.05) and with -0.378 < log2 (fold change) > 0.378]. Significantly (p < 0.05) enriched hits were then ranked in terms of activation status (Z-score). We additionally used IPA to compare the pathways significantly (p < 0.05) enriched in all the datasets, with predicted activation/inhibition in all the datasets, and with -1 < Z-score > 1 in at least one comparison, and same direction of modulation.

Flux balance analysis

Using R software packages SBMLR , BiGGR and sybil , we performed flux balance analysis (FBA) on HepatoNet1 , a manually reconstructed tissue-specific genome-scale metabolic model (GEM) for the hepatocyte. To perform FBA on our models, we first determined metabolic fluxes in the ''normal'' hepatocyte. Then, we mimicked the observed transcriptional changes for differentially expressed genes in each of the experimental set-ups (PH, CCl_4 and DEN/HFD), by increasing or decreasing the metabolic fluxes of the reactions catalysed by enzymes corresponding to the up- or down-regulated genes of interest. Further method details available in the Supporting Information.

RESULTS

Metabolic remodelling during proliferation and cancer

In order to elucidate the metabolic adaptations occurring in normal hepatocytes when they switch to proliferate, we used murine studies of compensatory regeneration following partial hepatectomy (PH) or acute toxic damage induced by carbon tetrachloride (CCl_4), and direct hyperplasia induced by phenobarbital (PB, an activator of the constitutive active androstane receptor (CAR). Seventy-two hours after the challenge, all the experimental models showed a substantial proportion of hepatocytes expressing the proliferating cell nuclear antigen (PCNA), suggesting that proliferative programs were activated in these cells at the time-point chosen (**Figure S1A-C**). Following CCl_4-treatment, there was extensive necrosis noted in pericentral areas, accompanied by increased inflammatory infiltrates (**Figure S1B**), whereas PB-treatment resulted in mild to moderate steatosis (**Figure S1C**), as shown before (24). To study proliferation in the context of HCC on a "lean" or fatty liver background, mice exposed to N-diethylnitrosamine (DEN) were maintained on either chow or high fat diet (HFD) (25).

Using Next Generation Sequencing (NGS) and Ingenuity Pathway Analysis (IPA), we studied the biological processes modulated in compensatory regeneration (PH and CCl_4) and HCC (DEN/HFD). As expected, we identified upregulation of pathways/bio-functions and upstream regulators associated with the regulation of cell cycle, survival, migration, invasion, and chromatin and extracellular matrix remodelling (**Supporting file 1**). In addition, upregulation of inflammation, angiogenesis, and other processes relevant for growth of multiple cancer types were identified.

IPA also predicted dysregulation of multiple canonical pathways and bio-functions involved in metabolism (**Figure 1A**), including the suppression of amino acid catabolism and inhibition of the nuclear receptor peroxisome proliferator-activated receptor α (PPARα; the master transcriptional regulator of hepatic fatty acid oxidation). Increased carbohydrate metabolism, and processes favouring the accumulation of lipids and cholesterol (which are needed for fueling proliferation;

Figure 1A) were also featured. Increased lipid synthesis was predicted in PH and DEN/HFD only, whilst increased oxidative stress featured only in models of hepatotoxicity and cancer (CCl_4 and DEN/HFD). Furthermore, suppression of fatty acid oxidation (and associated pathways) predominantly occurred in the CCl_4 model, but did not reach significance in PH and DEN/HFD models.

Next, we used IPA to study the activation status of upstream regulators (**Figure 1B-1C, Supporting file 1**). Interestingly, there was predicted activation of a number of nuclear receptors and their co-activators (e.g. Nrip1, Pxr, Rara, Ar, Vdr and the phospholipid sensor Lrh1 - previously described to control liver regeneration and HCC (8)); and of other crucial modulators of glucose and lipid metabolism. Predicted inhibited upstream regulators included nuclear receptors such as Hnf4a, the farsenoid X receptor (Fxr), as well as a plethora of other proteins involved in glucose and lipid metabolism, and negatively associated with cell proliferation and cancer (such as Pten, Hnf1a/b, Foxa1, Acox1 and Apoe). These results suggest that the rewiring of hepatocyte metabolism is orchestrated at transcriptional level, and that multiple factors are coherently modulated to allow the switch toward proliferation. In particular, changes to lipid and amino acid metabolism were indicated.

Proliferating hepatocytes are characterised by distinctive lipid composition

To investigate changes to lipid metabolism, we performed lipidomics experiments on models of compensatory regeneration (PH and CCl_4) and direct hyperplasia (PB). Proliferating liver tissue had distinct lipid profiles to their corresponding control group for all three models (**Figure 2A, Figure S2, Supporting file 2**). Using orthogonal projection to latent structures discriminant analysis (OPLS-DA; $R^2 = 0.89$, $Q^2 = 0.82$, $p < 0.001$), we found that samples undergoing compensatory regeneration had increased monounsaturated fatty acid (MUFA)-containing phosphatidylcholine (PC), phosphatidylethanolamine (PE) 40:6, short chain triacylglycerides (TAG) and free cholesterol, with a decrease in polyunsaturated fatty acid (PUFA)-containing PCs and sphingomyelin (SM) 40:1 (**Figure**

2B). On the other hand, direct hyperplasia following PB-treatment revealed a general increase in TAGs and cholesteryl esters (CE), increased MUFA-containing PC(36:1), and a decrease in PC(38:6) and PC(32:0), compared to control (OPLS-DA; $R^2 = 0.88$, $Q^2 = 0.87$, $p < 0.01$; **Figure 2C**). The increase in TAGs and cholesterol during proliferation is consistent with the transcriptional pathway analysis, which featured net accumulation of both lipid classes and suppressed fatty acid oxidation. However, the most striking observation was the significant increase in MUFA-containing PCs, that was consistent throughout the models of liver proliferation (**Figure 2D**). These results suggest that the increase in MUFA-containing PCs is a common event in hepatocyte proliferation, independent from the strategy used to switch on the proliferative program.

Monounsaturated phosphatidylcholine accumulates in HCC tumours

We next studied how the lipidome of HCC compares to adjacent non-tumour tissue in the DEN mouse models (in mice challenged with chow diet, or HFD to study hepatocellular carcinogenesis in the context of fatty liver). According to the lipid profiles measured using LC-MS (**Supporting file 2**) and analysed using principal components analysis (PCA), the four groups appeared to be well discriminated in terms of lipid composition, with samples split by diet in the first principal component (**Figure 3A**). A direct comparison of all tumour samples with non-tumour revealed that compared to their adjacent tissue, tumours had increased TAGs, CEs and MUFA-PC, and a decrease in PUFA-PC (OPLS-DA; $R^2 = 0.87$, $Q^2 = 0.71$, $p = 0.02$; **Figure 3B**). The levels of MUFA-PC were significantly increased in tumours for both DEN-exposed dietary groups at paired analysis (**Figure 3C**).

Despite accurately dissecting HCC tumours macroscopically, there still might be the risk of contamination of tumors with areas of normal tissue (and vice-versa). To independently confirm our data and overcome this potential limitation of whole-tissue lipid extractions, we used mass spectrometry imaging (MSI). MSI allows the spatial mapping of lipids across a tissue slice, and is therefore ideally suited for cancer research (12). Applying MSI to tissue sections, we confirmed a

striking accumulation of MUFA-PC and decrease in SM(40:1) in tumours of both chow and HFD models (**Figure 3D**). Furthermore, MSI highlighted the zonation of particular lipids across the non-tumour adjacent tissue, as we have shown previously (26) (**Figure 3E**).

As a further model of HCC, we employed a genetically-tractable mouse model of hepatocyte proliferation and spontaneous tumorigenesis. Concommitant activation of *Ras* and *Myc*, known oncogenes mutated or amplified in human HCC, resulted in rapid hepatocyte proliferation, and widespread formation of small and highly proliferative neoplasms. Taking advantage of the rapid and synchronous tumorigenesis in this model and the spatial lipid mapping potential of MSI, we investigated the lipidomic signature of these early cancerous lesions and of the surrounding tumor-free tissue. Similar to the DEN-induced tumours, we found an increase in MUFA-PC, particularly PC(34:1), in neoplastic lesions (**Figure 3F**), with documentable increased proliferation (**Figure S1D**).

Having established the major lipid profile changes in mouse models of proliferation and cancer, we sought to confirm whether these changes are also relevant in human HCC. Using a cohort of human HCC samples on a fatty liver background, we compared the lipid profiles in HCC compared to their paired non-tumour tissue (**Supporting file 2, Figure S3A**). This revealed an increase in MUFA-PC and decreased plasmalogens (HCC vs. HCC tissue; **Figure 4A**). Whilst the change in plasmalogens was not consistently recapitulated in the animal models (**Figure S3**), the increased MUFA-PC was in agreement with all the mouse models of proliferation and cancer. MSI was used to confirm these changes, revealing a particularly striking accumulation of MUFA-containing PC(36:1) in HCC (**Figure 4B**). These data further confirm that the increase in MUFA-containing PC is a crucial event, associated with the proliferative switch of hepatocytes and with hepatocellular carcinogenesis.

Metabolic reprogramming in liver regeneration and cancer

Next, we measured a set of core aqueous metabolites (**Supporting file 3**). Metabolite profiles measured during liver regeneration (PH and CCl_4-treated) were clearly distinguishable from their

corresponding control profiles, whilst PB-treatment did not result in a significantly different metabolite profile compared to control (**Figure S4A**). We then went on to identify the metabolites responsible for differentiating liver regeneration from control groups (OPLS-DA; $R^2 = 0.97$, $Q^2 = 0.87$, $p < 0.01$; **Figure S4B**). Overall liver regeneration following PH or CCl_4-injury resulted in significantly increased levels of many amino acids (e.g. glutamate, proline, leucine), increased metabolites involved in phospholipid biosynthesis (e.g CDP-choline), and nucleotide intermediates (ribose-5-phosphate, cytidine).

For the metabolite profiles of DEN-treated mice, we found that the samples were differentiated by diet on the first principal component (**Figure S4C**). The DEN/chow tumour samples were separated from non-tumour in the second principal component however the separation between tumour and non-tumour was poor for DEN/HFD, when looking at aqueous metabolite profiles alone (**Figure S4C**). Further study of the DEN/chow group (OPLS-DA; $R^2 = 0.98$, $Q^2 = 0.90$, $p = 0.02$; **Figure S4D**) suggested that tumours had increased amino acids (e.g. glutamate and glutamine) and citric acid cycle (TCA) intermediates (malate, succinate, citrate, fumarate), compared to non-tumour tissue. Tumours were also characterised by decreased β-hydroxybutyrate (**Figure S4D**) – a by-product of mitochondrial β-oxidation, in agreement with the inhibited action of PPARα from the transcriptomics pathway analysis.

Lastly, we measured the aqueous metabolite profiles for human HCC and associated non-tumour tissue. We found several amino acids to be significantly increased in HCC tumours, including lysine, histidine and alanine; whereas aspartate was significantly reduced (**Supporting file 3**). Critically, similar to the liver regeneration studies, there was a significant increase in CDP-choline in HCC versus non-tumour tissue (**Figure 4C**).

Overall our metabolomics results are in-line with proliferating cells undergoing metabolic rewiring to sustain a higher demand for macromolecular biosynthesis of amino acids, phospholipids and nucleotides, and increased energy production. In particular, proliferating cells have an increased

need for glucogenic amino acids (such as glutamine/glutamate) in order to supply nitrogen and carbon for biosynthesis and to produce ATP via the TCA cycle. The observed increase in amino acids may be driven, at least in part, by the suppression of their catabolism, as highlighted by transcriptional pathway analysis.

Metabolic fluxes are directed towards increased phospholipid synthesis

Metabolomics and lipidomics experiments demonstrated an increase in MUFA-containing PC and CDP-choline during liver regeneration and cancer. Using gene expression data from the same PH, CCl_4 and DEN/HFD samples, we performed a targeted analysis of the main metabolic pathways involved in the generation and homeostasis of MUFA-PC (**Figure 5**), using differential gene expression patterns. Where multiple isoforms of a gene are involved in a reaction (e.g. *Dgat1*, *Dgat2*), we considered only those that were significantly different in at least one of the three models. We validated our findings *in silico*, by performing flux balance analysis (FBA) on a genome-scale metabolic model (GEM) of the hepatocyte (**Table S3**).

Starting with catabolic pathways, and in agreement with the pathway analysis featuring suppressed PPARα activity (**Figure 1B**), there was an overall trend across the three groups for decreased expression of genes and reduced metabolic flux for mitochondrial (*Acads, Acadsb, Cpt2*) and peroxisomal β-oxidation (*Acox1*, *Acox3*) pathways (**Figure 5A, Table S3**). Activation of FFA to fatty acyl-CoA prior to oxidation is carried out by the long chain acyl-CoA synthetases (ACSL). Whilst expression for *Acsl1* was consistently decreased across the groups, that of *Acsl4* and *Acsl5* were consistently increased. Though not exclusive, these three enzymes have been shown to have substrate preference for MUFA, PUFA and saturated fatty acids (SFA), respectively (27, 28). It is therefore tempting to speculate that during times of rapid proliferation, whilst β-oxidation is reduced overall, PUFA and/or SFA are oxidised in preference to MUFA.

Turning to anabolic pathways (**Figure 5B**), we found increased gene expression and/or metabolic flux for lipogenic genes (e.g. *Acaca, Acly*), and the elongation (*Elovl6*) and desaturation (*Scd1/2*) of palmitic acid, FFA(16:0), to FFA(18:1), particularly in the PH and DEN/HFD models. Fatty acids can then be incorporated into PC via the Land's cycle (*Lpcat*). Metabolic fluxes suggest that the Land's cycle is working towards the synthesis of phospholipids (**Table S3**).

PC is also formed *de novo* via the Kennedy pathway (**Figure 5C**). This pathway was upregulated in proliferation and cancer, through increased gene expression of *Chka* and availability of substrate (e.g. choline). Furthermore, breakdown of SM can also contribute phosphocholine, a substrate which can enter the Kennedy pathway (**Figure 5C**). This is supported by increased gene expression of *Smpd3*, and MSI which showed a dramatic decrease of SM(40:1) in tumours (**Figure 3D**). FBA confirmed that the Kennedy pathway is driven towards increased PC synthesis in hepatocyte proliferation and cancer (**Table S3**).

In addition, following the imposed up/down regulations of the fluxes through β-oxidation and lipogenesis, the whole metabolic network reacts by enhancing lipid synthesis and modulating flux through both glycolysis (*e.g*. upregulated commitment and rate-limiting steps catalysed by hexokinase, Hk, and phosphofructokinase, Pfk) and the TCA cycle (upregulated at the level of citrate synthase, Cs; downregulated at malate dehydrogenase, Mdh*,* and α-ketoglutarate dehydrogenase, Ogdh*,* steps; **Table S3**), thus working as an anaplerotic pathway for *de novo* lipogenesis.

MUFA lipids are correlated with genetic markers of hepatocellular carcinoma

Having identified potential lipid metabolic pathways affected by proliferation and cancer, we next evaluated gene/metabolite correlations in tumour-only groups to see if their concentration correlated with the proliferative behaviour. Within DEN/HFD tumours, we assessed correlation of total MUFA-PC with related lipid metabolic genes, and with known diagnostic and prognostic markers of HCC. We found a strong positive correlation between total MUFA-PC and *Chka, Acly,*

Scd2, Lpl, Acsl4 gene expression and choline, CDP-choline metabolites (**Figure S5**). This suggests that the increase in MUFA-PC in tumours is closely linked to *de novo* lipogenesis, desaturation by *Scd* and synthesis of PC by the Kennedy pathway. On the other hand, a strong negative correlation was observed between MUFA-PC and *Acsl1, Pemt, Dgat2* and *Acad* gene expression. In addition, MUFA-PC was positively correlated to proliferation markers (*Ki67, Ccne1, Ccnd1, Ccne2, Ccnd2*), and HCC diagnostic markers (*Afp, Spp1*), thus suggesting the importance of these lipids for the proliferative status of HCC (**Figure S5**).

Lastly, we performed RNA sequencing on human HCC tumours to assess whether similar correlations would also be found. We performed a Spearman's rank correlation analysis for the three groups of PC (SFA, MUFA, PUFA) and related lipid genes, with gene expression pertaining to known markers of HCC and proliferation. There were several clusters identified in the correlation matrix for HCC tumours, whereas no clusters and few significant correlations could be calculated within the non-tumour group (**Figure 6A, Figure S6**). Similar to the DEN/HFD model, we found distinct associations for MUFA-PC in tumours, compared to SFA- and PUFA-containing PC. Considering the lipid-related pathways, MUFA-PC was positively correlated with gene expression for ACLY, *ACACA*, *ELOVL6, SCD,* and *ACSL4;* and with CDP-choline metabolite levels. There was positive correlation of SFA-PC with *LAMB1, ICAM1, TGFB1* (markers of EMT, amongst other functions), and *CCND2*. As previously described in murine samples, MUFA-PC was associated with expression of proliferation and cell cycle markers (*CCNE2, CCNA2, CCNB2, PCNA, MYC*), and several clinical diganostic and/or prognostic markers of HCC (e.g. *AFP, SPP1*) (**Figure 6A, Figure 6B**).

Taken together, our data suggest that hepatocyte proliferation in HCC is linked to: *i*) enhanced *de novo* lipogenesis; *ii*) increased SCD-mediated desaturation of fatty acyl chains; *iii*) reduced β-oxidation; and *iv*) increased *de novo* synthesis of PC through the Kennedy pathway. This has the net result of increasing the MUFA pool, and MUFA-PC in particular. MUFA-PC may therefore have use as a marker of proliferation, and warrants further large-scale studies to assess the suitability of these

lipids for clinical application as diagnostic and prognostic biomarkers of HCC or, for use of MUFA-PC anabolic pathways as targets for treatment.

DISCUSSION

Growing evidence suggests that the modulation of cell metabolism could be a good strategy to ameliorate cell proliferation in cancer. It is of great importance, therefore, to unravel the complex metabolic adaptations arising in cancer cells, when they switch to uncontrolled proliferation. This may lead to identifying novel pharmacological targets and potential diagnostic or prognositc biomarkers. Several metabolomics studies on HCC have been performed to date (29-32). Here we show for the first time an integrated systems biology dataset (lipids, aqueous metabolites and RNA sequencing), studying the reprogramming of lipid metabolism in multiple models of liver regeneration, direct hepatic hyperplasia, and in murine and fatty liver-associated human HCC.

The most striking difference amongst models of proliferation was that PB-treated mice developed a substantially higher hepatic TAG content than other models, as expected (33). In the murine models of HCC, there were distinct differences in the TAG composition, with a greater increase in short-chain TAGs in tumours of the HFD model, compared to chow (**Figure S7**). This highlights diet-specific changes in hepatic metabolism, in the context of HCC. Importantly, we were also able to identify the changes in lipid metabolism occurring in proliferating hepatocytes, independently from the challenge that activates the proliferative program, or of the surrounding microenvironment.

Specifically, an increase in MUFA-PC was measured by lipidomics, and confirmed by MSI in cancer, for all the models. We integrated data from lipidomics, metabolomics and transcriptomics to link these changes in lipid content to specific pathways. These included increased lipogenesis, fatty acyl desaturation, *de novo* synthesis of PC, PC remodelling and decreased β-oxidation. We also show for the first time that levels of MUFA-PC are strongly correlated with proliferation markers, cell cycle

control and other known genetic markers of HCC in both mouse and human tumours. Increased MUFA in the lipidome may confer several advantages to highly proliferative cancer cells and has been described before (34-36). One such advantage would be to prevent an accumulation of palmitic acid from increased lipogenesis, which otherwise could trigger endoplasmic reticulum (ER) stress and apoptoic signalling pathways (37). Furthermore, a reduction in saturated phospholipids was reported to alter membrane fluidity in HCC cells, resulting in improved uptake of glucose and increased metastatic abilities (38). Reducing PUFA in the PC fraction could also help proliferating cells to ameliorate the production of pro-inflammatory eicosanoids via phospholipase action, thereby promoting cell survival and the priming of proliferative programs. The decreased plasmalogens observed in HCC, compared to non-tumour tissue, is also of interest. A subset of these lipids are thought to play a protective role against oxidative damage and depleted levels of circulating plasmalogens have been linked to HCC (decreased in serum of HCC patients compared to control group) and type 2 diabetes (32, 39-41).

Targeting lipid metabolism is increasingly attracting interest as a therapeutic strategy for HCC (42). There is a growing body of evidence suggesting that inhibition of the desaturation and elongation of fatty acids offers an alternative to suppressing *de novo* synthesis (37, 43-45). Our study suggests that the change in the abundance of multiple lipid-related metabolic genes is associated with the development and progression of human HCC and warrant further study to evaluate their potential as drug targets. Since hepatic MUFA-PC was closely correlated with proliferation and other markers of HCC, this further has the potential to become a new prognostic marker and enable improved patient stratification.

Finally, our study revealed that much of the lipid reprogramming in cancer cells was also recapitulated in mouse models of liver regeneration and direct hepatic hyperplasia, suggesting that these mechanisms are not necessarily cancer-specific but more broadly associated with hepatocyte proliferation. This has important implications to better understand the role of lipid metabolism in

the pathophysiological events linking NASH-cirrhosis to HCC but also in terms of personalised medicine. Given that hepatocyte proliferation is impaired in advanced phases of chronic liver disease, our study suggests that the choice of metabolic target for the treatment of HCC might need careful evaluation, particularly when associated with liver resection. Overall, our study has shed new light on metabolic adaptions of proliferating hepatocytes to enrich MUFA-PC, opening several new avenues for future research and highlighting the power of integrating data from multiple –omics techniques.

REFERENCES

1. Malato Y, Naqvi S, Schürmann N, Ng R, Wang B, Zape J, Kay MA, et al. Fate tracing of mature hepatocytes in mouse liver homeostasis and regeneration. The Journal of Clinical Investigation 2011;121:4850-4860.
2. Allaire M, Nault JC. Type 2 diabetes–associated hepatocellular carcinoma: A molecular profile. Clinical Liver Disease 2016;8:53-58.
3. Sanyal AJ, Yoon SK, Lencioni R. The etiology of hepatocellular carcinoma and consequences for treatment. Oncologist 2010;15 Suppl 4:14-22.
4. Cancer Genome Atlas Research Network. Electronic address wbe, Cancer Genome Atlas Research N. Comprehensive and Integrative Genomic Characterization of Hepatocellular Carcinoma. Cell 2017;169:1327-1341.e1323.
5. Teilhet C, Morvan D, Joubert-Zakeyh J, Biesse A-S, Pereira B, Massoulier S, Dechelotte P, et al. Specificities of Human Hepatocellular Carcinoma Developed on Non-Alcoholic Fatty Liver Disease in Absence of Cirrhosis Revealed by Tissue Extracts ^{1}H-NMR Spectroscopy. Metabolites 2017;7:49.
6. Vacca M, Allison M, Griffin JL, Vidal-Puig A. Fatty acid and glucose sensors in hepatic lipid metabolism: Implications in NAFLD. Seminars in Liver Disease 2015;35:250-261.
7. Anstee QM, Reeves HL, Kotsiliti E, Govaere O, Heikenwalder M. From NASH to HCC: current concepts and future challenges. Nature Reviews Gastroenterology & Hepatology 2019.
8. Vacca M, Degirolamo C, Massafra V, Polimeno L, Mariani-Costantini R, Palasciano G, Moschetta A. Nuclear receptors in regenerating liver and hepatocellular carcinoma. Molecular and Cellular Endocrinology 2013;368:108-119.
9. Griffin JL, Lehtimäki KK, Valonen PK, Gröhn OHJ, Kettunen MI, Ylä-Herttuala S, Pitkänen A, et al. Assignment of 1H Nuclear Magnetic Resonance Visible Polyunsaturated Fatty Acids in BT4C Gliomas Undergoing Ganciclovir-Thymidine Kinase Gene Therapy-induced Programmed Cell Death. Cancer Res 2003;63:3195-3201.
10. Hilvo M, Denkert C, Lehtinen L, Muller B, Brockmoller S, Seppanen-Laakso T, Budczies J, et al. Novel theranostic opportunities offered by characterization of altered membrane lipid metabolism in breast cancer progression. Cancer Res 2011;71:3236-3245.
11. Gaude E, Frezza C. Tissue-specific and convergent metabolic transformation of cancer correlates with metastatic potential and patient survival. Nature Communications 2016;7:13041.
12. Hall Z, Ament Z, Wilson CH, Burkhart DL, Ashmore T, Koulman A, Littlewood T, et al. Myc expression drives aberrant lipid metabolism in lung cancer. Cancer Research 2016;76:4608-4618.

13. Baenke F, Peck B, Miess H, Schulze A. Hooked on fat: the role of lipid synthesis in cancer metabolism and tumour development. Dis Model Mech 2013;6:1353-1363.
14. Rohrig F, Schulze A. The multifaceted roles of fatty acid synthesis in cancer. Nat Rev Cancer 2016;16:732-749.
15. Vacca M, Degirolamo C, Massafra V, Polimeno L, Mariani-Costantini R, Palasciano G, Moschetta A. Nuclear receptors in regenerating liver and hepatocellular carcinoma. Mol Cell Endocrinol 2013;368:108-119.
16. Caldez MJ, Van Hul N, Koh HWL, Teo XQ, Fan JJ, Tan PY, Dewhurst MR, et al. Metabolic Remodeling during Liver Regeneration. Developmental Cell 2018;47:425-438.e425.
17. Huang J, Rudnick DA. Elucidating the metabolic regulation of liver regeneration. The American journal of pathology 2014;184:309-321.
18. Piccinin E, Peres C, Bellafante E, Ducheix S, Pinto C, Villani G, Moschetta A. Hepatic peroxisome proliferator-activated receptor gamma coactivator 1beta drives mitochondrial and anabolic signatures that contribute to hepatocellular carcinoma progression in mice. Hepatology 2018;67:884-898.
19. Vacca M, D'Amore S, Graziano G, D'Orazio A, Cariello M, Massafra V, Salvatore L, et al. Clustering Nuclear Receptors in Liver Regeneration Identifies Candidate Modulators of Hepatocyte Proliferation and Hepatocarcinoma. PLOS ONE 2014;9:e104449.
20. Higgins GM. Experimental pathology of the liver. Restoration of the liver of the white rat following partial surgical removal. AMA Arch Pathol 1931;12:186-202.
21. Murphy DJ, Junttila MR, Pouyet L, Karnezis A, Shchors K, Bui DA, Brown-Swigart L, et al. Distinct thresholds govern Myc's biological output in vivo. Cancer cell 2008;14:447-457.
22. Jackson EL, Willis N, Mercer K, Bronson RT, Crowley D, Montoya R, Jacks T, et al. Analysis of lung tumor initiation and progression using conditional expression of oncogenic K-ras. Genes Dev 2001;15:3243-3248.
23. Folch J, Lees M, Stanley GHS. A simple method for the isolation and purification of total lipids from animal tissues. Journal of Biological Chemistry 1957;226:497-509.
24. Massart J, Begriche K, Moreau C, Fromenty B. Role of nonalcoholic fatty liver disease as risk factor for drug-induced hepatotoxicity. Journal of clinical and translational research 2017;3:212-232.
25. Santos NP, Colaco AA, Oliveira PA. Animal models as a tool in hepatocellular carcinoma research: A Review. Tumour Biol 2017;39:1010428317695923.
26. Hall Z, Bond NJ, Ashmore T, Sanders F, Ament Z, Wang X, Murray AJ, et al. Lipid zonation and phospholipid remodeling in nonalcoholic fatty liver disease. Hepatology 2017;65:1165-1180.
27. Grevengoed TJ, Klett EL, Coleman RA. Acyl-CoA metabolism and partitioning. Annual review of nutrition 2014;34:1-30.
28. Yan S, Yang X-F, Liu H-L, Fu N, Ouyang Y, Qing K. Long-chain acyl-CoA synthetase in fatty acid metabolism involved in liver and other diseases: an update. World journal of gastroenterology 2015;21:3492-3498.
29. Huang Q, Tan Y, Yin P, Ye G, Gao P, Lu X, Wang H, et al. Metabolic characterization of hepatocellular carcinoma using nontargeted tissue metabolomics. Cancer Res 2013;73:4992-5002.
30. Muir K, Hazim A, He Y, Peyressatre M, Kim DY, Song X, Beretta L. Proteomic and lipidomic signatures of lipid metabolism in NASH-associated hepatocellular carcinoma. Cancer Res 2013;73:4722-4731.
31. Patterson AD, Maurhofer O, Beyoglu D, Lanz C, Krausz KW, Pabst T, Gonzalez FJ, et al. Aberrant lipid metabolism in hepatocellular carcinoma revealed by plasma metabolomics and lipid profiling. Cancer Res 2011;71:6590-6600.
32. Lu Y, Chen J, Huang C, Li N, Zou L, Chia SE, Chen S, et al. Comparison of hepatic and serum lipid signatures in hepatocellular carcinoma patients leads to the discovery of diagnostic and prognostic biomarkers. Oncotarget 2018;9:5032-5043.
33. Wada T, Gao J, Xie W. PXR and CAR in energy metabolism. Trends Endocrinol Metab 2009;20:273-279.

34. Guo S, Wang Y, Zhou D, Li Z. Significantly increased monounsaturated lipids relative to polyunsaturated lipids in six types of cancer microenvironment are observed by mass spectrometry imaging. Sci Rep 2014;4:5959.
35. Bansal S, Berk M, Alkhouri N, Partrick DA, Fung JJ, Feldstein A. Stearoyl-CoA desaturase plays an important role in proliferation and chemoresistance in human hepatocellular carcinoma. J Surg Res 2014;186:29-38.
36. Budhu A, Roessler S, Zhao X, Yu Z, Forgues M, Ji J, Karoly E, et al. Integrated metabolite and gene expression profiles identify lipid biomarkers associated with progression of hepatocellular carcinoma and patient outcomes. Gastroenterology 2013;144:1066-1075 e1061.
37. Peck B, Schulze A. Lipid desaturation - the next step in targeting lipogenesis in cancer? FEBS J 2016;283:2767-2778.
38. Lin L, Ding Y, Wang Y, Wang Z, Yin X, Yan G, Zhang L, et al. Functional lipidomics: Palmitic acid impairs hepatocellular carcinoma development by modulating membrane fluidity and glucose metabolism. Hepatology 2017;66:432-448.
39. Jang JE, Park HS, Yoo HJ, Baek IJ, Yoon JE, Ko MS, Kim AR, et al. Protective role of endogenous plasmalogens against hepatic steatosis and steatohepatitis in mice. Hepatology 2017;66:416-431.
40. Dean JM, Lodhi IJ. Structural and functional roles of ether lipids. Protein Cell 2018;9:196-206.
41. Oresic M, Simell S, Sysi-Aho M, Näntö-Salonen K, Seppänen-Laakso T, Parikka V, Katajamaa M, et al. Dysregulation of lipid and amino acid metabolism precedes islet autoimmunity in children who later progress to type 1 diabetes. The Journal of experimental medicine 2008;205:2975-2984.
42. Lally JSV, Ghoshal S, DePeralta DK, Moaven O, Wei L, Masia R, Erstad DJ, et al. Inhibition of Acetyl-CoA Carboxylase by Phosphorylation or the Inhibitor ND-654 Suppresses Lipogenesis and Hepatocellular Carcinoma. Cell Metabolism 2019;29:174-182.e175.
43. Peck B, Schug ZT, Zhang Q, Dankworth B, Jones DT, Smethurst E, Patel R, et al. Inhibition of fatty acid desaturation is detrimental to cancer cell survival in metabolically compromised environments. Cancer Metab 2016;4:6.
44. Su Y-C, Feng Y-H, Wu H-T, Huang Y-S, Tung C-L, Wu P, Chang C-J, et al. Elovl6 is a negative clinical predictor for liver cancer and knockdown of Elovl6 reduces murine liver cancer progression. Scientific Reports 2018;8:6586.
45. Shibasaki Y, Horikawa M, Ikegami K, Kiuchi R, Takeda M, Hiraide T, Morita Y, et al. Stearate-to-palmitate ratio modulates endoplasmic reticulum stress and cell apoptosis in non-B non-C hepatoma cells. Cancer Sci 2018;109:1110-1120.

AUTHOR CONTRIBUTIONS

ZH, MV and JLG conceived and designed the study and wrote the manuscript. MV, JL, ES, LP, QMA, GIE, AVP, and FO designed and performed the animal experiments. MA and MH provided human samples and data. ZH, EC and GM performed lipidomics and metabolomics analyses. DC, ZH and MV performed the statistical, bioinformatics and pathway analyses. All the authors provided useful criticism during the study, and critically reviewed the manuscript.

ACKNOWLEDGEMENTS

The authors are indebted to the following, who supported the activities presented in this manuscript: Dr Olivier Govaere (Newcastle University); Dr James West (University of Cambridge); the Disease Model Core, the Genomics and Transcriptomics Core, the Histology Core and the Imaging Core at Metabolic Research Laboratories, University of Cambridge; staff in the Genomics Core Facility (GCF) and the Bioinformatic Support Unit (BSU; Peter Leary & Simon J. Cockell) at Newcastle University. The human samples come from the Human Research Tissue Bank of the Cambridge University Hospitals, which is supported by the NIHR Cambridge Biomedical Research Centre.

DATA AVAILABILITY

All the data are available upon request. NGS data in this manuscript has been deposited on GEO data repository (GSE140463 and GSE140243).

FIGURE LEGENDS

Figure 1. Pathway enrichment analysis of the transcriptome reveals changes to metabolism of lipids and amino acids in proliferation and cancer. Enrichment analysis for canonical pathways (CP) and bio-functions (BF) was performed on differentially expressed genes for the PH (N = 5), CCl_4 (N = 3) and DEN/HFD (N = 4) models (**A**). Comparative analysis of predicted upstream regulators (UR) for PH (N = 5), CCl_4 (N = 3) and DEN/HFD (N = 4) models, based on pathways significantly ($p < 0.05$) enriched and with a predicted activation/inhibition (predicted activation status: Z-score) (**B**). "Network-like" graphical representation of the interaction between upstream regulators and the differentially modulated pathways they control (blue: downregulated; orange: upregulated) in the three models (**C**). Full list of modulated pathways in Supporting File 1 (BF: n44; CP: n15; UR: n191).

Figure 2. **Mice undergoing hepatocyte proliferation have characteristically different hepatic lipid profiles to controls.** Lipid profiles were measured by liquid chromatography mass spectrometry (LC-MS), and compared using partial least squares discriminant analysis (PLS-DA) (**A**). Orthogonal (O)PLS-DA models and their associated S-plots were constructed to compare liver regeneration (PH and CCl_4) groups versus control (**B**), and direct hyperplasia PB-treated versus control (**C**). There was consistently an increase in monounsaturated (MUFA)-containing phosphatidylcholines (PC) in proliferating liver (**D**). Paired data are represented as spaghetti plots; non-paired data show mean ± SEM (*** $p < 0.001$, ** $p < 0.01$, * $p < 0.05$). PH experiment (before = 5, after = 5); CCl_4 experiment (control = 3, treated = 3); PB experiment (control = 5, treated = 6).

Figure 3. MUFA-containing PC is increased in tumours for different models of HCC. HCC was induced by DEN-exposure in WT mice, fed a chow or high fat diet (HFD). LC-MS based lipidomics data were used to perform principal components analysis (PCA) and to construct PLS-DA models, wherein good separation of the different groups was achieved (**A**). OPLS-DA was used to compare tumour-containing groups versus non-tumour groups (**B**). There was an increase in MUFA-containing PC in tumour for DEN/HFD and DEN/chow mice (**C**). Paired data are shown as spagetti plots (*** $p < 0.001$,

** $p < 0.01$, * $p < 0.05$). DEN/chow: N = 4 per group; DEN/HFD: N = 6 per group. Mass spectrometry imaging (MSI) revealed that MUFA-containing PC is increased, and SM(40:1) is decreased, in tumours for three different models of HCC. Adjacent H&E stained sections are shown, alongside single ion intensity images (**D**). An overlay of three lipid distributions, highlighting the differentiation of tumour from adjacent, zonated tissue (representative sample from the DEN/chow group is shown) (**E**). The spatial distribution of PC(34:1) in control tamoxifen-treated liver is contrasted to that following oncogenic activation of MYC (**F**). In control, PC(34:1) follows a zonal pattern correpsonding to periportal areas, as reported previously; following activation of MYC, the zonation is altered with PC(34:1) co-localising with neoplastic lesions.

Figure 4. Lipid and metabolite changes in human hepatocellular carcinoma. Increased MUFA-PC and decreased plasmalogens were found in HCC tumours, compared to non-tumour (**A**). MSI shows increased MUFA-containing PC(36:1) in human HCC, compared to adjacent non-tumour tissue (**B**). Aqueous metabolomics experiments revealed a striking increase in CDP-choline in tumours, compared to non-tumour (**C**). Paired data are shown;*** $p < 0.001$, ** $p < 0.01$, * $p < 0.05$); N = 7.

Figure 5. Multi-omics reveals widespread modulation of lipid metabolism in liver proliferation and cancer. Gene expression and metabolic fluxes were examined for pathways involved in β-oxidation (**A**), *de novo* lipogenesis (**B**) and synthesis of PC by the Kennedy pathway (**C**). For lipid catabolism, genes of interest included fatty acid activation (*Acsl* family), carnitine shuttle (*Cpt2*), mitochondrial (*Acad* family) and peroxisomal (*Acox* family) β-oxidation, and ketogenesis (*Aacs*). Acetyl-coA from β-oxidation can enter the TCA cycle, which generates citrate for lipid synthesis. Fatty acids are synthesised by *de novo* lipogenesis (*Acly*, *Acaca, Fasn*), and subsequently elongated (*Elovl6*) and desaturated (*Scd*). They can then be esterified into complex lipids, such as phosphatidylcholine (PC) by the Land's cycle (*Lpcat*). PC is also formed *de novo* by the Kennedy pathway (*Chka, Pcyt1, Chpt1*). Dietary lipids (hydrolysis of TAGs by *Lpl*) and sphingomyelin (breakdown by *Smdp3*) can also feed into the Kennedy pathway. Finally, phosphatidylethanolamine (PE) can be converted to PC by *Pemt*.

Predicted metabolic flux for the PH model is indicated by colour of the enzyme names (red = upregulated; blue = downregulated) (**A**). Individual gene expression log2 fold changes after PH (N = 5), CCl_4-treatment (N = 3) and in DEN/HFD (N = 4) tumours are shown in adjacent heatmaps. *** $p < 0.001$, ** $p < 0.01$, * $p < 0.05$, adjusted for false discovery using Benjamin-Hochberg approach. Legend for heat map shown at bottom. Supporting file 4 and Table S3 have further details on the metabolic flux analysis.

Figure 6. MUFA-PC is correlated with proliferation, cell cycle and markers of HCC in humans. Heatmap of correlation matrix (Spearman's rank correlation coefficient, 95 % C.I., $p < 0.05$ adjusted using Benjamin-Hochberg method) for gene expression and differentially unsaturated PCs in human HCC tumours (N = 7). Metabolites are in yellow text; lipid-related genes in green and HCC-associated genes in blue. Two main clusters were identified. The first shows a positive correlation of SFA-PC to several genes associated with HCC. The second cluster links MUFA-PC to proliferation and further HCC-associated genes. In addition, MUFA-PC was positively correlated with lipid metabolic genes *ELOVL6, SCD, ACSL4, ACACA* and metabolite CDP-choline (**A**). Individual patient correlations for *PCNA, CCNE2* and *CCNB2* gene expression with MUFA-PC concentration, and *TGFB1* with SFA-PC (**B**).

Figures

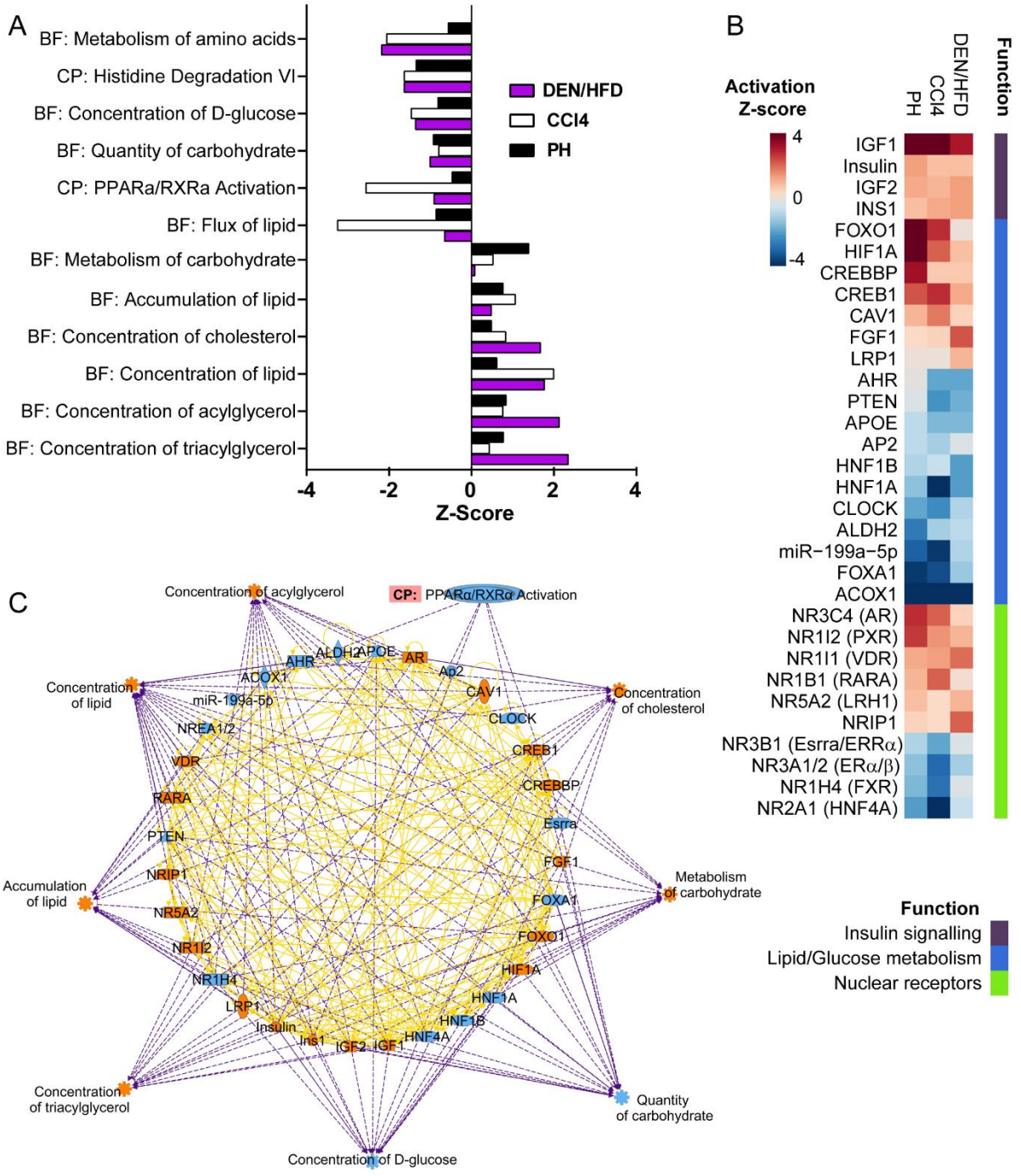

Figure 1

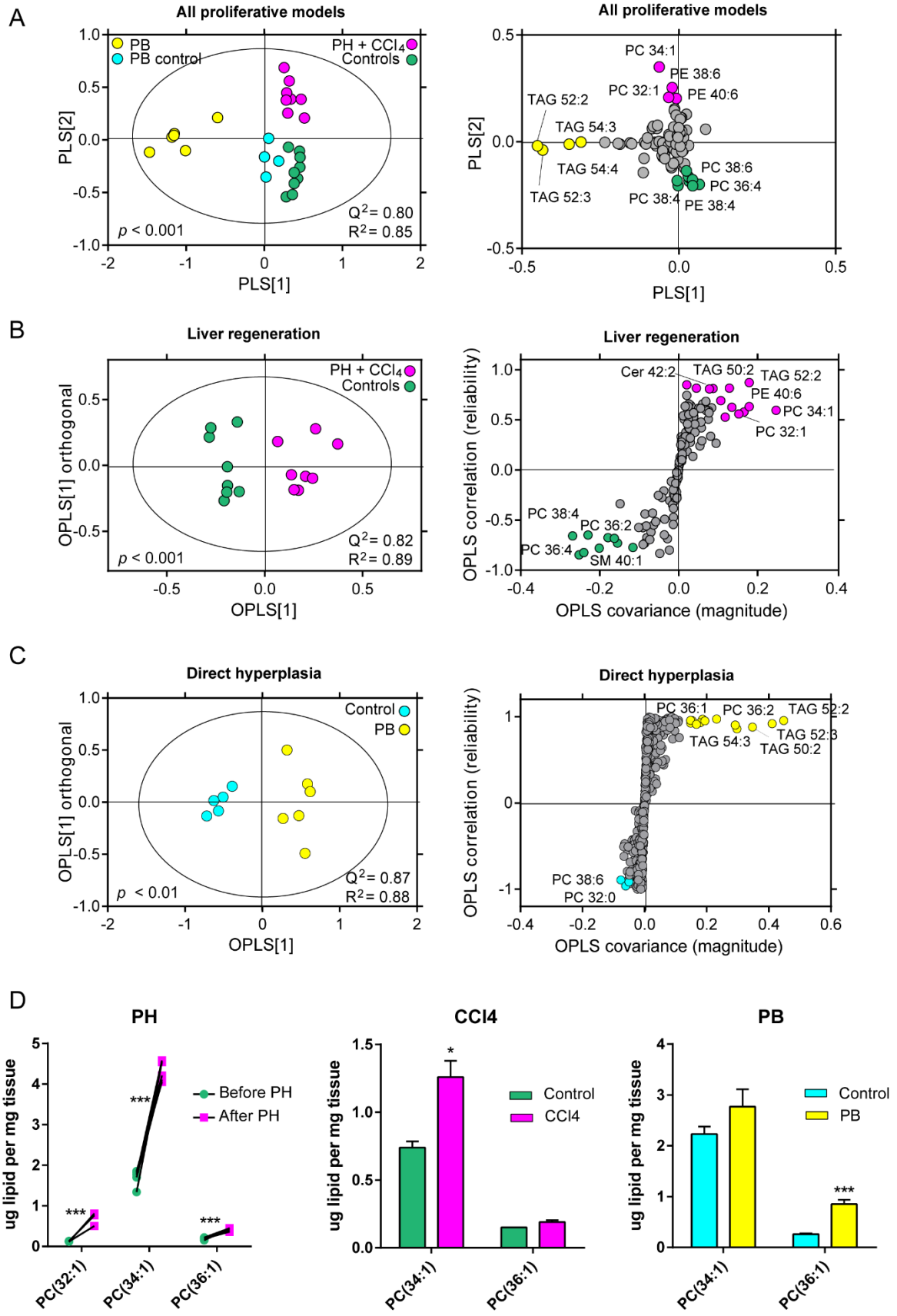
A
All proliferative models
PB
PB control
PH + CCl4
Controls
PLS[2]
PLS[1]
p < 0.001
Q2= 0.80
R2= 0.85
All proliferative models
PC 34:1
PE 38:6
PC 32:1
PE 40:6
TAG 52:2
TAG 54:3
TAG 54:4
TAG 52:3
PC 38:6
PC 36:4
PC 38:4
PE 38:4
PLS[2]
PLS[1]
B
Liver regeneration
PH + CCl4
Controls
OPLS[1] orthogonal
OPLS[1]
p < 0.001
Q2= 0.82
R2= 0.89
Liver regeneration
Cer 42:2
TAG 50:2
TAG 52:2
PE 40:6
PC 34:1
PC 32:1
PC 38:4
PC 36:2
PC 36:4
SM 40:1
OPLS correlation (reliability)
OPLS covariance (magnitude)
C
Direct hyperplasia
Control
PB
OPLS[1] orthogonal
OPLS[1]
p < 0.01
Q2= 0.87
R2= 0.88
Direct hyperplasia
PC 36:1
PC 36:2
TAG 52:2
TAG 52:3
TAG 54:3
TAG 50:2
PC 38:6
PC 32:0
OPLS correlation (reliability)
OPLS covariance (magnitude)
D
PH
Before PH
After PH
ug lipid per mg tissue
PC(32:1)
PC(34:1)
PC(36:1)
CCl4
Control
CCl4
ug lipid per mg tissue
PC(34:1)
PC(36:1)
PB
Control
PB
ug lipid per mg tissue
PC(34:1)
PC(36:1)

Figure 2

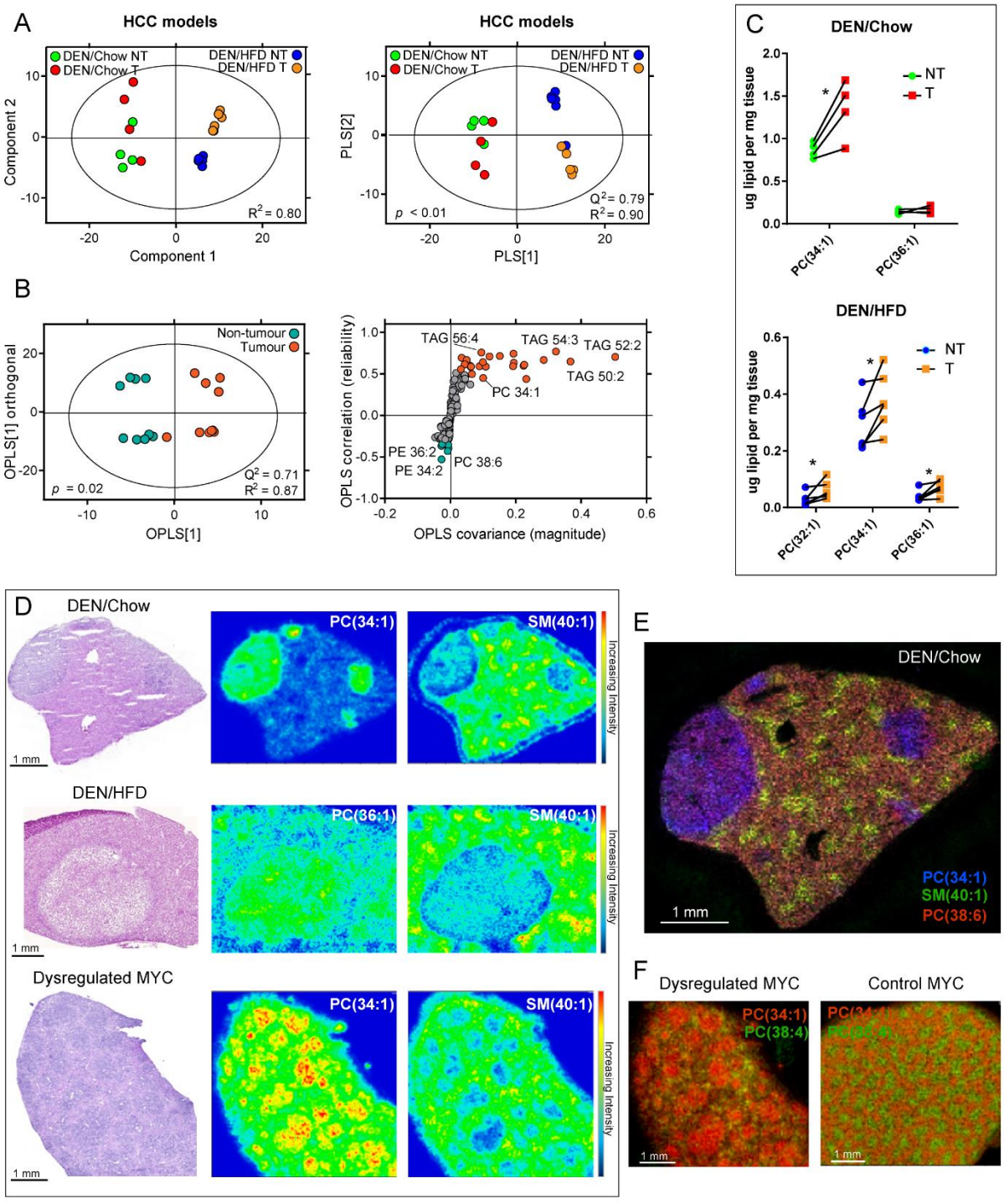
A
HCC models
DEN/Chow NT
DEN/Chow T
DEN/HFD NT
DEN/HFD T
Component 2
Component 1
R² = 0.80
HCC models
PLS[2]
PLS[1]
p < 0.01
Q² = 0.79
R² = 0.90
B
Non-tumour
Tumour
OPLS[1] orthogonal
OPLS[1]
p = 0.02
Q² = 0.71
R² = 0.87
OPLS correlation (reliability)
OPLS covariance (magnitude)
TAG 56:4
TAG 54:3
TAG 52:2
TAG 50:2
PC 34:1
PE 36:2
PE 34:2
PC 38:6
C
DEN/Chow
ug lipid per mg tissue
NT
T
PC(34:1)
PC(36:1)
DEN/HFD
PC(32:1)
PC(34:1)
PC(36:1)
D
DEN/Chow
PC(34:1)
SM(40:1)
Increasing Intensity
1 mm
DEN/HFD
PC(36:1)
SM(40:1)
Dysregulated MYC
E
DEN/Chow
PC(34:1)
SM(40:1)
PC(38:6)
F
Dysregulated MYC
Control MYC
PC(34:1)
PC(38:4)

Figure 3

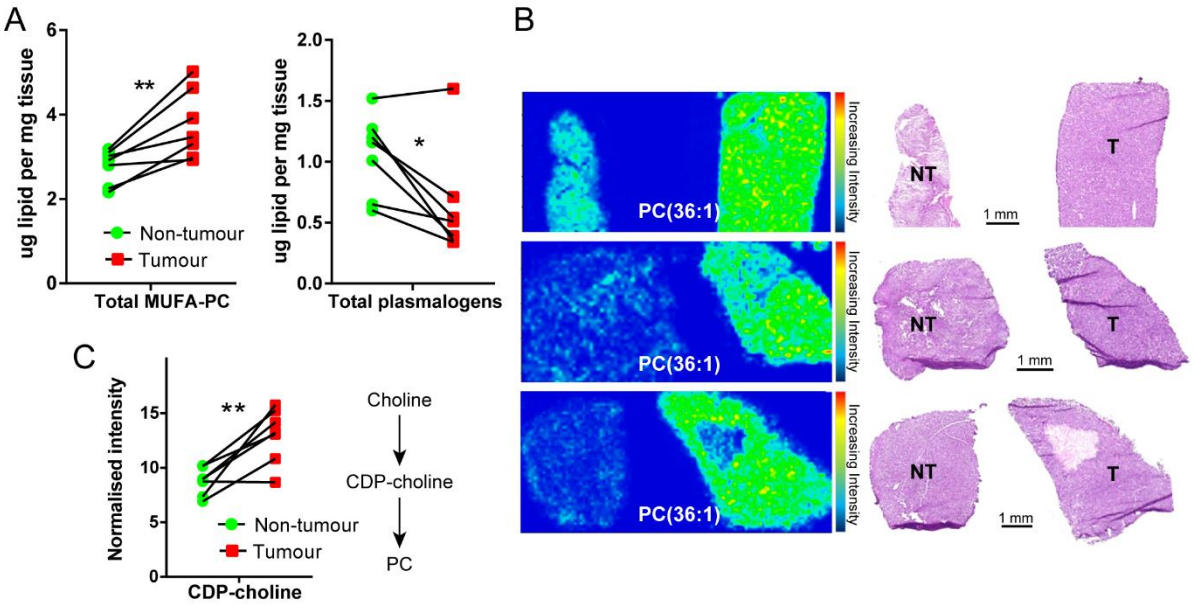
A
ug lipid per mg tissue
**
Non-tumour
Tumour
Total MUFA-PC
*
Total plasmalogens
B
PC(36:1)
Increasing Intensity
NT
T
1 mm
C
Normalised intensity
CDP-choline
Choline
PC

Figure 4

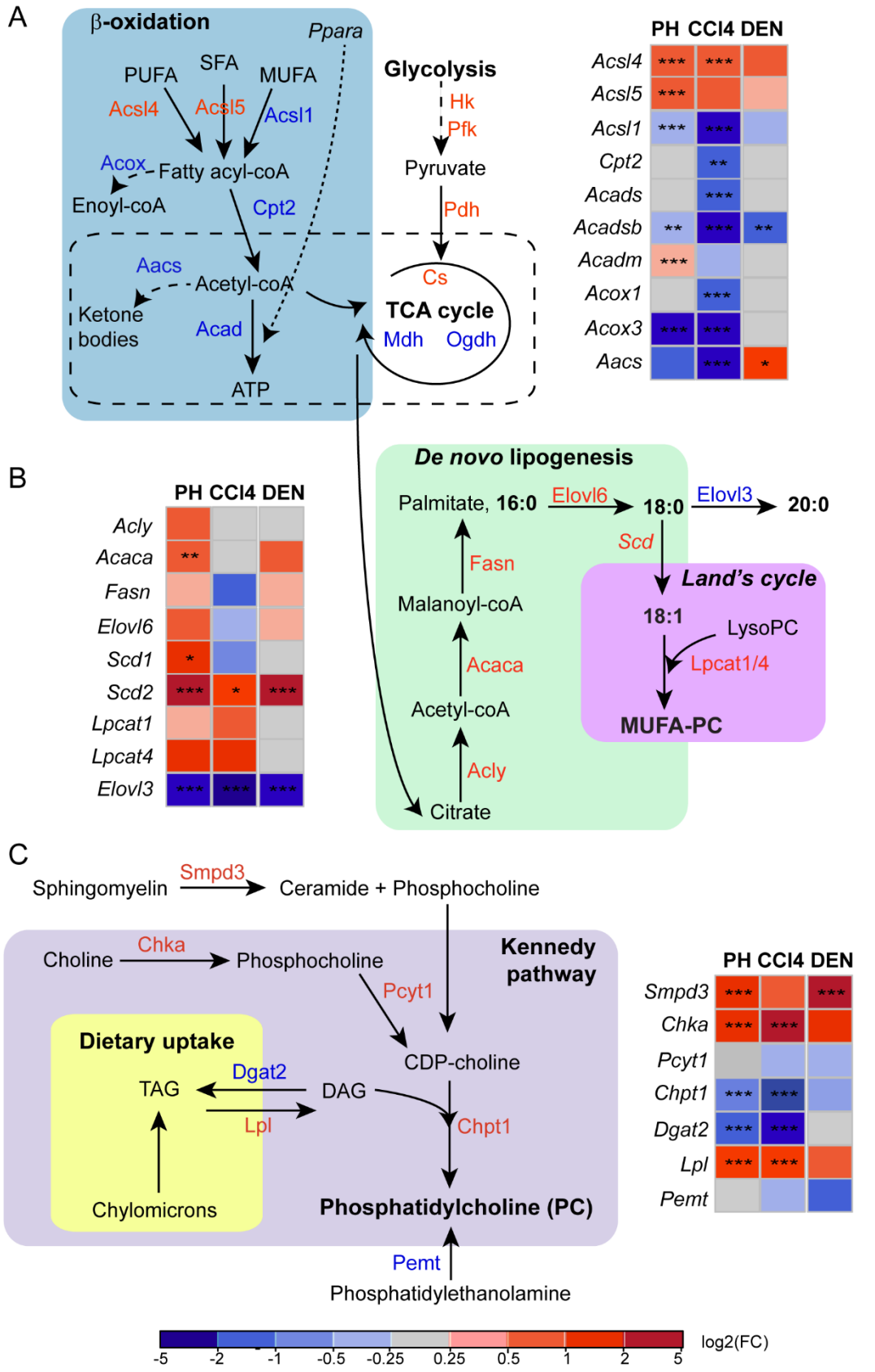
A
β-oxidation
Ppara
PUFA
SFA
MUFA
Acsl4
Acsl5
Acsl1
Acox
Fatty acyl-coA
Enoyl-coA
Cpt2
Aacs
Acetyl-coA
Ketone bodies
Acad
ATP
Glycolysis
Hk
Pfk
Pyruvate
Pdh
Cs
TCA cycle
Mdh
Ogdh
PH CCl4 DEN
Acsl4
Acsl5
Acsl1
Cpt2
Acads
Acadsb
Acadm
Acox1
Acox3
Aacs
B
PH CCl4 DEN
Acly
Acaca
Fasn
Elovl6
Scd1
Scd2
Lpcat1
Lpcat4
Elovl3
De novo lipogenesis
Palmitate, 16:0
Elovl6
18:0
Elovl3
20:0
Scd
Land's cycle
18:1
LysoPC
Lpcat1/4
MUFA-PC
Fasn
Malanoyl-coA
Acaca
Acetyl-coA
Acly
Citrate
C
Sphingomyelin
Smpd3
Ceramide + Phosphocholine
Choline
Chka
Phosphocholine
Kennedy pathway
Pcyt1
CDP-choline
Dietary uptake
TAG
Dgat2
DAG
Lpl
Chpt1
Chylomicrons
Phosphatidylcholine (PC)
Pemt
Phosphatidylethanolamine
PH CCl4 DEN
Smpd3
Chka
Pcyt1
Chpt1
Dgat2
Lpl
Pemt
log2(FC)
-5
-2
-1
-0.5
-0.25
0.25
0.5
1
2
5

Figure 5

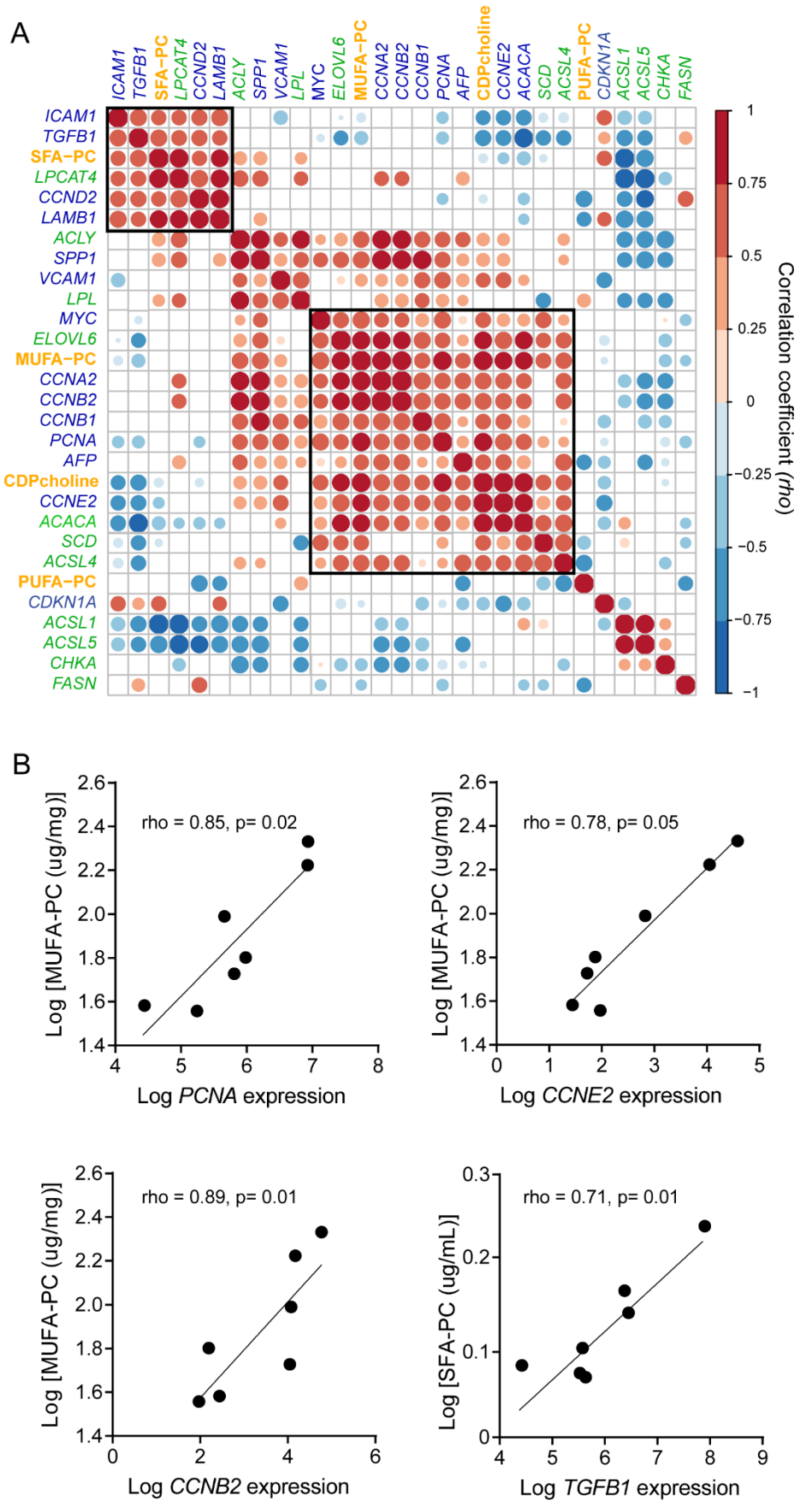
A
ICAM1
TGFB1
SFA−PC
LPCAT4
CCND2
LAMB1
ACLY
SPP1
VCAM1
LPL
MYC
ELOVL6
MUFA−PC
CCNA2
CCNB2
CCNB1
PCNA
AFP
CDPcholine
CCNE2
ACACA
SCD
ACSL4
PUFA−PC
CDKN1A
ACSL1
ACSL5
CHKA
FASN
1
0.75
0.5
0.25
0
−0.25
−0.5
−0.75
−1
Correlation coefficient (rho)
B
rho = 0.85, p= 0.02
Log [MUFA-PC (ug/mg)]
Log PCNA expression
rho = 0.78, p= 0.05
Log [MUFA-PC (ug/mg)]
Log CCNE2 expression
rho = 0.89, p= 0.01
Log [MUFA-PC (ug/mg)]
Log CCNB2 expression
rho = 0.71, p= 0.01
Log [SFA-PC (ug/mL)]
Log TGFB1 expression

Figure 6